Note: This is an in-press pre-proof peer-reviewed draft of the journal article:

Price, S., Vamvakeros, A., Jacques, S., Beale, A. et al., “μ-CT Investigation into the Impact of a Fuel-Borne Catalyst Additive on the Filtration Efficiency and Backpressure of Gasoline Particulate Filters,” SAE Int. J. Fuels Lubr. 15(2):2022, doi:10.4271/04-15-02-0006.

ISSN: 1946-3952

DOI: https://doi.org/10.4271/04-15-02-0006

Available online 18th January 2022 at: https://saemobilus.sae.org/content/04-15-02-0006/

20XX-01-XXXX

μ-CT Investigation into the Impact of a Fuel Borne Catalyst Additive on the Filtration Efficiency and Backpressure of Gasoline Particulate Filters

Stephen W.T. Price,[1] Antonis Vamvakeros,[1] Simon D.M. Jacques,[1] Andrew M. Beale,[2,3]

Kathryn E. Rankin,[4] Nathan Hollingsworth,[5] David Coultas,[5] and Amy Challinor[5]

[1]Finden Ltd., UK

[2]Department of Chemistry, University College London, UK

[3]Research Complex at Harwell, UK

[4]University of Southampton, UK

[5]Infineum UK Ltd., UK

Abstract

An investigation into the pre-ashing of new gasoline particulate filters has demonstrated that the filtration efficiency of such filters can be improved by up to 30% (absolute efficiency improvement) when pre-conditioned using ash derived from a fuel borne catalyst additive. The additive is typically used in diesel applications to enable diesel particulate filter regeneration and can be added directly into the fuel tank of the vehicle. This novel result was compared with ash derived from lube oil componentry, which has previously been shown to improve filtration efficiency in gasoline particulate filters. The lube oil-derived ash utilised in this work improved the filtration efficiency of the gasoline particulate filter by ~30%, comparable to the ash derived from the fuel borne catalyst additive. The undesirable impact of the ash deposit on backpressure increases was also investigated, and it was established that the use of the fuel borne catalyst additive resulted in a lower backpressure increase versus the equivalent ash loading from lube oil components. Following the real world vehicle testing and gasoline particulate filter evaluation, the used, intact filters were further analysed, using micro-focus computed tomography (μ-CT) to assess the ash distribution within the filters. It was established that the fuel borne catalyst-derived ash was predominantly deposited near the outlet plug region of the filter, whereas the lube oil-derived ash was also distributed within the channel walls, which resulted in a higher GPF back pressure. The μ-CT results were therefore key to establish the differences between these two ash providing sources and enabled a better understanding of the effect of filter microstructure on macroscopic performance, i.e. gasoline particulate filter efficiency and backpressure results.

Introduction

The Gasoline Particulate Filter

Legislation concerning exhaust emissions from passenger cars has become increasingly rigorous since the introduction of Euro 1 in 1992. Diesel engines were the initial focus of legislation to limit particulate emissions, with the introduction of the diesel particulate filter (DPF) enabling compliance. More recently, the progressively stringent limitations have led to increased focus on the particulate emissions from gasoline direct injection (GDI) engines and the development of the gasoline particulate filter (GPF). GDI engines have significantly gained in popularity in recent years due to the fuel economy benefits these engines can provide in comparison to the port fuel injection (PFI) alternative; however the particulate emissions from GDI engines are typically higher than those from PFI engines [1 – 4].

A GPF accomplishes the same function as a DPF, trapping particles (carbonaceous or ‘soot’ deposits formed during the incomplete combustion of hydrocarbon fuels) and thus preventing them escaping with the exhaust gas emissions [5]. However, a more limited fundamental and practical understanding of the GPF exists, and there are several challenges unique to their application that need to be addressed to ensure successful GPF use: the limitation of backpressure increase, the achievement of suitable filtration efficiency, the use of suitable substrate materials, the GPF size and position in the after-treatment system and the potential use of catalytic coatings. This study explores the effect of a fuel borne catalyst (FBC) additive on backpressure and filtration efficiency.

GPF Filtration Efficiency

There are key differences between the particulate emissions from diesel and GDI engines; the typical engine-out particulate emissions are much lower from a GDI engine compared to a diesel engine, and the average particle size is smaller [3]. This fundamental difference in soot loading and morphology impacts the initial filtration efficiency of the GPF, as it takes considerably longer for a layer of soot to build within the filter. DPF filtration efficiency levels of >98% can be achieved relatively quickly in a new, fresh filter, owing to the formation of this 'soot cake'. For the GPF however, the initial filtration efficiency of a fresh filter can be as low as ~50%. This could potentially cause issues as vehicles must comply with emissions legislation following a specified homologation period.

It has been established that the introduction of a small amount of ash within the GPF enables the filtration efficiency to be significantly improved compared to the new, bare filter substrate, by forming an additional filtration barrier [6 - 10]. Ash from lubricant oil will collect within the filter during the vehicle's lifetime, however this is gradual and may not significantly impact filtration efficiency during the homologation phase. One study into the use of lubricant oil to improve the filtration efficiency of new GPFs had demonstrated that small amounts of ash, around 2.5 g/L (grams per litre of GPF volume), can increase the filtration efficiency by >10% [6]. To achieve this, fully formulated experimental engine oils (SAE 5W-20 viscosity grade) were artificially introduced via direct injection into the combustion chamber, at a 2% doping level in the gasoline fuel.

A separate study examining GPF filtration efficiency found that ash levels, created through fuel doping with contaminants to mimic lube oil ash build up over time, of up to 3 g/L can provide an improved filtration efficiency from approximately 60% to 80%, with minimal impact (20 – 33% increase) on backpressure [7].

Lube oil ash build up during typical vehicle use occurs at a much slower rate than the artificially doped examples referenced, and the vehicle would have to be driven for thousands of kilometers before reaching a 2 – 2.5 g of ash per litre loading [9, 10]. Therefore, GPF filtration efficiency can be low for a significant portion of the vehicles initial use, potentially before the homologation period has ended. Adding lube oil components directly to the fuel brings the disadvantages of introducing potential catalyst poisons into the exhaust gas after-treatment system, and the high artificial doses that are required to build an initial GPF ash layer are not recommended for typical vehicle use [11 – 14].

X-ray Computed Tomography

X-ray micro-focus computed tomography (µ-CT) is increasingly used to provide insight into intact, functional devices, and can do so over a range of length scales [5, 14 – 18]. This non-destructive, volumetric imaging technique has previously been used to study filters both ex situ [10, 19 - 21], and under in situ conditions, for example the recent study by Jones et al. used time resolved synchrotron µ-CT to image the blocking of individual pores by TiO_2 nanoparticles within cut sections of wall flow filters [5]. It is even possible to obtain advanced chemical information by combining CT with scattering and spectroscopic methods, such as X-ray diffraction (XRD-CT) [22, 23], or X-ray fluorescence (XRF-CT) [24]. These combined tomographic approaches can reveal minor chemical contributions and spatial heterogeneities within intact devices that would otherwise be missed by conventional measurements.

Other recent studies have used microscopy and tomography to look at various filter types including sintered metal fiber filters [21, DPFs [25, 26] and GPFs [20]. However, in these cases the authors looked at small sub sections, ranging from 1-4 channels, either removed from the filters post testing, or measured under idealized conditions in the laboratory. This approach allows for higher resolution to be obtained, and also for chemical mapping through the use of EDX (Kamp, Yang), providing insight into the blocking of individual pores within the channel walls. However, the field of view of these studies is limited with respect to the total filter size, and the conditions are still highly controlled, and so do not account for the greater range of conditions that are encountered when filters are used in real world conditions.

The work reported here is intended to be a step towards understanding filter performance under real world conditions, and the influence of potentially beneficial additives such as FBCs, moving from highly controlled laboratory studies to real world driving conditions. Whilst these conditions inevitably are less controlled due to factors such as variable environmental conditions, the outcomes from the study still provide valuable information on the factors which affect GPF filtration efficiency and backpressure, and how additives such as FBCs can provide improvements.

GPF Commissioning Studies

The aim of this investigation was to establish whether the use of a fuel borne catalyst (FBC) additive could provide rapid ash loading in a GPF, and therefore enable a filtration efficiency improvement. The results were compared to the equivalent ash loading from lube oil components. The impact on backpressure that the additional filter ash provided was also assessed for both FBC and lube-derived ash. It was anticipated that the use of a fuel additive to improve filtration efficiency could mitigate some of the disadvantages that arise when adding lube oil components directly to the fuel or within the fuel system, such as the increased concentration of potential catalyst poisons (metals such as zinc and phosphorous) [11 – 13].

A fuel borne catalyst is typically employed to enable DPF regeneration (soot combustion) at lower temperatures (vs. the uncatalysed regeneration), and these additives typically make use of an iron and/or cerium metal oxide as the active catalyst [27 - 33]. FBC additives have been used commercially for this application for over a decade, enabling effective DPF regeneration without any undesired impact to the vehicle.

In this study, we compared the use of the FBC additive with the equivalent amount of lube-derived ash, to establish the impact on new

GPFs. Following this, lab-based µ-CT was conducted on the series of complete GPFs to investigate the effect of ash loading on the channel, wall and plug regions under real world operating conditions, and to determine how the FBC additive impacts filtration efficiency and backpressure.

Experimental

GPF Test Method

All % filtration improvements are absolute, not relative, throughout the paper.

A series of three newly manufactured, unused gasoline particulate filters from the same manufacturing batch were subjected to a three-stage test regime (Table 1).

Table 1: Test regime for GPFs

Stage	Description
1 – Baseline efficiency	The three new, unused GPFs were individually measured for filtration efficiency and exhaust backpressure on an engine dynamometer set-up. This represented the baseline filter function for new filters at the start of the test. The GPFs were regenerated before and after these measurements, to ensure that any carbon/soot particles had no impact on the results. (see Appendix Table S1)
2 – Commissioning	The filters were each installed in a GDI passenger car exhaust system, which was then operated to consume a single tankful of gasoline fuel. The test fuel composition was varied for each filter to allow the effect of the treated fuel to be compared with untreated fuel (see below commissioning process information). For the real driving part of the assessment, the same driving route was used for each GPF.
3 – Final assessment	The filters were removed from the vehicle and replaced in the dynamometer set-up of stage 1, to measure filtration efficiency (see Appendix Table S2) and exhaust backpressure. Comparison of the results from stage 1 and stage 3 illustrated the impact of ash loading. Again, as in Stage 1, the GPFs were regenerated before and after these measurements, to ensure the filters were free of soot. (see Appendix Table S1)

Each GPF was subjected to a different commissioning process, the details of which are in Table 2. We anticipate no soot loading was present at the time of filtration efficiency measurements (Table 1, Stage 1 and Stage 3), due to the regeneration steps (see Appendix Table S1).

Table 2: Commissioning process for GPFs

GPF	Commissioning
1 - Baseline (no fuel additive)	Full tank (68 L) of standard gasoline used to assess impact on new GPF (baseline)
2 - FBC treated fuel	To the full tank of standard gasoline, FBC additive (stabilized iron oxide colloid) was added to target 3 g/L ash (ash comprising iron oxide)
3 - Lube oil componentry treated fuel	To the full tank of standard gasoline, lube oil additive components were added to target 3 g/L ash (ash comprising calcium oxide)

The lube oil componentry that was added to the fuel matched that used in the vehicles' lubricant system. The gasoline used in all three stages was equivalent (Aral Super Plus RON 98). The orientation of the filters and direction of exhaust flow are shown in Figure 1.

The lube oil and FBC dosing into the fuel tank were calculated to provide 3 g/L of ash in the GPF. The vehicle was driven over the same route using a full fuel tank to condition each filter. Due to the small differences in the GPF weights before and after testing, it was not practical to weigh the 'before and after' GPFs. The absolute difference would be too small to be reliable vs. the GPF weight, and water condensation would also impact the result if the filter was hot following regeneration (which would be required to ensure any soot weight was not taken into account). Further details on the commissioning studies are provided in the SI.

µ-CT Characterisation

The three filters (GPF 1 – 3) from the vehicle testing were assessed by µ-CT scanning (see Appendix Table S3 for µ-CT scanning parameters). To enable this analysis, at the end of the bench test assessments each filter was regenerated to remove any carbon build-up and to ensure only ash deposits remained.

Overview scans were first conducted on the filters in a custom dual source 225/450 kVp Hutch CT scanner (Nikon Metrology, UK) using a micro-focus 225 kVp source with a tungsten reflection target and a Perkin Elmer XRD 1621 CN03 HS detector, at 234.4 µm voxel (cubic pixel) resolution (234 mm width field of view (FOV)). Region of interest (ROI) scans of the inlet and outlet channels were then carried out using a modified 225 kVp Nikon/X-tek HMX µ-CT scanner (Nikon metrology, UK) at 32.1 µm voxel resolution (64 mm width FOV). An additional overview scan with 70.3 µm voxel resolution (140 mm width FOV) of GPF 2 and 3 was conducted in the custom Hutch. All overview scans were performed with the filters orientated

normal to the X-ray beam, whilst ROI scans were performed with the filters tilted ca. 30° to the beam.

Data was reconstructed into 32 bit float raw volumes using the filtered back-projection FDK implemented within CTPro3D and CTAgent v2.2 (Nikon Metrology, UK), and the intensities were normalised across all datasets to allow for direct comparison of values e.g. density. The reconstructed data was processed with MATLAB to re-orient the tilted ROI scans back to normal. ImageJ [34] was used for depth profile analysis of the overview scans, and Avizo (Thermo Fisher Scientific), was used for image segmentation of the ROIs to provide quantification of the channel and plug regions at the inlet and outlet of all GPFs. The channels of all three filters were segmented using Avizo, and their individual volumes calculated. As the height of the sub-volumes used for the segmentation is known, and the channels may be taken to be square, the average channel widths could therefore be computed and compared to give an indicator of the degree of ash build up. Since there are incomplete channels at the edges of each sub-volume, the data were filtered to extract only the largest 200 channels from each dataset to ensure an equal number of channels from each dataset was available. Additional 3D rendering was performed using Drishti 35].

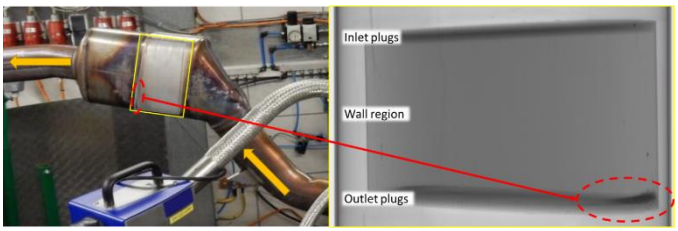

Figure 1: (Left) Orientation of exhaust during testing with gas flow highlighted by yellow arrows. Within this canning was only the GPF, the three-way catalyst was not present on the dynamometer investigations. (Right) Radiograph of GPF 2 with 70.3 µm resolution inlet is towards top of image, gas flow direction and outlet are towards bottom. Dense particulate accumulation is visible on bottom right of filter, also small amount in bottom left. Note: filter orientation during radiograph collection is 90° rotated from use.

Results

From stage 1, the initial filtration efficiency of each GPF was recorded (Table 3). This was compared directly to the efficiency found in stage 3. In all of the GPFs, an increase in filtration efficiency was achieved after the commissioning stage (stage 2), however GPFs 2 and 3 had larger delta (% improvement) corresponding to the targeted addition of 3 g/L ash. It was found that both ash from the FBC additive and lube oil were consistently comparable and provided significant improvements in GPF filtration efficiency. Data is based on > 23 nm particle number measurements.

The initial and final filtration efficiencies in Table 3 are averaged over two runs (see Table S2 for further information). The increases observed for filtration efficiency for a given filter, and differences between filters, are greater than the error of the repeated measurements, and therefore are considered to be significant.

Table 3: Filtration efficiency improvement data at each operating point assessed. Filtration efficiency was calculated using: ((particulate number before GPF – particulate number after GPF)/particulate number before GPF)*100%.

Operating Point 1			
GPF	Initial Filtration Efficiency (stage 1)	Final Filtration Efficiency (stage 3)	Increase
1	51%	58%	7%
2	47%	78%	31%
3	48%	80%	32%
Operating Point 2			
GPF	Initial Filtration Efficiency (stage 1)	Final Filtration Efficiency (stage 3)	Increase
1	65%	73%	8%
2	63%	89%	26%
3	63%	92%	29%
Operating Point 3			
GPF	Initial Filtration Efficiency (stage 1)	Final Filtration Efficiency (stage 3)	Increase
1	71%	79%	8%
2	71%	93%	22%
3	68%	95%	27%

It was observed that GPF 1, despite there being no additional ash source added, had an average increase in filtration efficiency of 7% across the three steady state operating points assessed. Ash will naturally accumulate in the GPF due to fuel combustion and the presence of lube oil ash. Thus we hypothesize that this increase is due to the natural accumulation of ash material in the filter and is related to the fuel and lube oil used during this study.

Operating point 1 was also evaluated to provide a comparison of the backpressure for each GPF, before and after the commissioning stage (Table 4). It was found that GPF 2, which had been commissioned with the FBC additive, had a lower backpressure increase of 9.5 mbar compared to GPF 3, where lube oil ash had been introduced to the filter and the backpressure rose by 23.4 mbar. This indicates that along with the reduced impact on the overall vehicle system, the fuel borne catalyst additive can also provide a reduced impact on the backpressure, thus minimising the trade-off between filtration efficiency and vehicle operation.

Table 4: Comparison of backpressure in the GPFs assessed at Operating Point 1.

Operating Point 1			
GPF	(stage 1) Initial Backpressure (mbar)	(stage 3) Final Backpressure (mbar)	Delta (mbar)
1	96.2	96.7	0.5
2	96.5	106.0	9.5
3	97.6	121.0	23.4

Overall, it was demonstrated that a low loading of the FBC-derived ash (3 g/L) can improve the filtration efficiency of a new GPF and is comparable to that of the known literature for the use of lube oil components for the same (2.5 g/L providing >10% efficiency improvements) [6].

Quantification by µ-CT

Overview scan depth profile analysis

Initial radiographs of the filters showed GPF 2 to have high density particulates collected in the bottom of the filter channels, with a greater concentration on one side. This location is indicative of the bend in the inlet piping to the filter, i.e. as the exhaust enters the filter, it does so off-center (Figure 1). The heavier particulate matter in the exhaust travels the shortest distance across the filter, settling in the base of the nearest channels, as illustrated in the rendering of the reconstructed data (Figure 2). This particulate deposition is not observed in GPF 1 or GPF 3. GPF 2 also exhibits an orange discolouration across the inlet indicative of iron oxide deposition.

For the depth profile analysis of the filters a congruent region of the 3 overview scans was used; the average intensity of each layer of the reconstructed volume was summed, to give plots of the average intensity as a function of height (Figure 3). A region external to each filter was also profiled to provide a background intensity value. Given the intensity of all 3 datasets was normalised during processing, comparison of these depth profile plots may be used to indicate differences such as plug deposition or channel wall deposition to evaluate the effectiveness of the FBC additive in reducing the backpressure of the filter and increasing its useable lifetime.

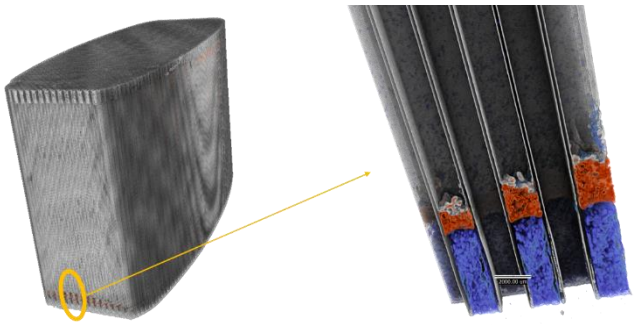

Figure 2: µ-CT rendering of GPF 2, highlighting the channel walls (grey) channel plugs (blue) and iron oxide ash (red). Left hand side is 70.3 µm overview, right hand side is close up from 32.1 µm ROI scan.

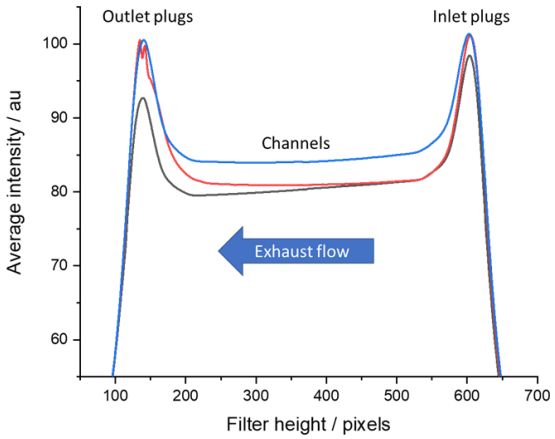

Figure 3: Depth profile analysis of GPF 1 (black, baseline), GPF 2 (red) and GPF 3 (blue)

The average intensity (i.e. density) of all three filters is higher at the inlet than the outlet, both for the peak associated with plug regions (higher intensity due to half of the channels being filled) and also the channel walls in between. This variation is most pronounced in the 'ash free' baseline GPF 1, indicating that it may be a physical feature originating during the filter production. There is a ca. 4% increase in the average intensity of the GPF 3 inlet and along the channel walls, increasing to ca. 8% at the outlet; indicating that ash build up occurs over the whole filter, but is found predominantly towards the outlet. In contrast, whilst the use of the FBC additive also causes ca. 4% increase in the average intensity at the inlet, this rapidly drops off once past the plug region and the channel wall intensities are comparable with those of the baseline filter (GPF 1). Towards the base of the channels by the outlet plug region there is ca. 3% increase in average intensity, whilst the outlet region increases between 6 – 8%. There is a more complex variation in the intensity in this region due to the iron oxide ash that has accumulated in the base of the filter. The increase observed in the inlet region for GPF 2 may be caused, at least in part, by the deposition of the FBC additive, given the visible discolouration. With the inlet and outlet regions having similar intensities, it appears that the FBC additive is most effective in reducing the deposits in the channel wall regions, with the plug regions having similar intensity caused by

comparable ash build up within the plugs. Correlating the average densities of these regions with the filtration and backpressure efficiencies reported in Tables 3 and 4, indicates that filtration efficiency is more greatly affected by the porosity of the plug regions, whilst backpressure is influenced by the wall porosity. Thus, we hypothesize that the cracks in the GPF plug region provide a more accessible route for the exhaust gas to pass out of the filter. Therefore, although only a small portion of the filter volume, a cracked plug will provide the easier 'free path' for gas to flow, versus crossing the wall and leaving the filter by the intended route. By filling the plug regions with ash, wall filtration becomes the only option for exhaust gas to pass out of the filter, therefore ensuring all of the exhaust gas is filtered and subsequently improving filtration efficiency of the GPF.

Examination of each cross-sectional reconstructed image of the filters as a function of height shows a greater intensity in the centre of the filter than at the edges, i.e. the channel walls of the filters begin to block in the middle of the filter. Comparison of any two like-for-like large regions from the overview scans consistently shows a higher intensity in the channel region for GPF 3 (i.e. density/ash deposition than for GPF 2). This indicates that the exhaust gas flow is greatest through the centre of the filter, as is no doubt intended. There is a subtle diagonal variation to this intensity distribution, correlated with the position of the inlet piping, that may be attributed to a mass-sensitive time-of-flight distribution; the larger heavier particles travel a shorter distance across the filter, being trapped in the near-lower section, whilst the lightest particles are blown further across the top of the filter inlet, being trapped in the far-upper section (Figure 1).

Region of Interest (ROI) Analysis

Manufacturing tolerances of the filters were observed in the µ-CT, for example, there was higher intensity (density) at the inlet region of the filters, the channel structures are not perfectly parallel, and there were micro-cracks in the plug regions. These features and trends were consistent across all three filters imaged, and so deviations or relative changes from these were used to assess the extent of ash deposition, and the subsequent impact on filtration efficiency and backpressure.

Following the tilt correction of the ROI scans a 20 x 20 x 20 mm sub-volume was extracted for further analysis, encompassing the plug region and a ca. 16 mm length of channels which were fully bound, i.e. it did not extend to cover any volume outside of the GPF and had all 4 walls intact. The plug region included in this sub-volume covered from the inner edge (i.e. start of the plug) up to the edge of the filter – but stopped ca. 50 µm just before the outer edge. Between 225-279 fully bound channels were in each sub-region and were used to describe and compare the dimensions of the channels. With regards to the plug region in the sub-volume, ca. 136 plugs were present, and used to analyse and compare features such as the porosity.

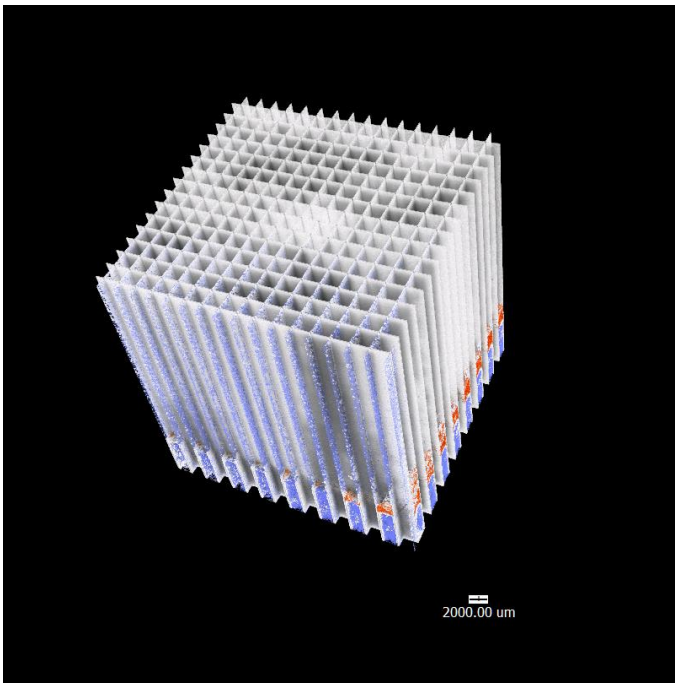

Figure 4: Example of sub-volume extracted from GPF outlet region. Volume is 20 x 20 x 20 mm; scale bar is 2 mm. Channel walls (grey) channel plugs (blue) and iron oxide ash (red).

Avizo was used to segment the channels, the deposited material within the channels, as well as the pores and cracks in the plug regions. The datasets were thresholded, labelled and a marker-based watershed approach used to separate each channel and enable filtering and analysis by volume and location. A rendered image of the outlet region of GPF 2 is shown in Figure 4.

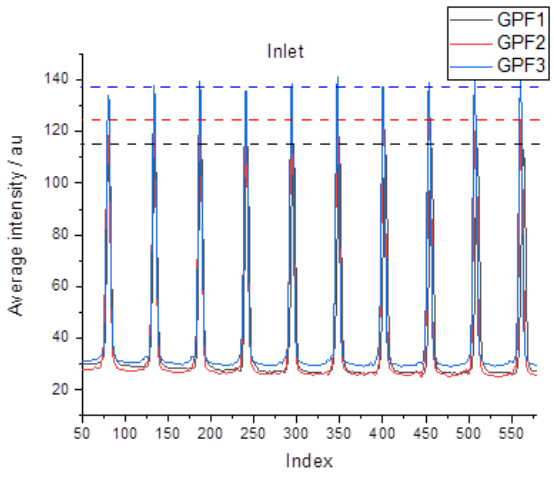

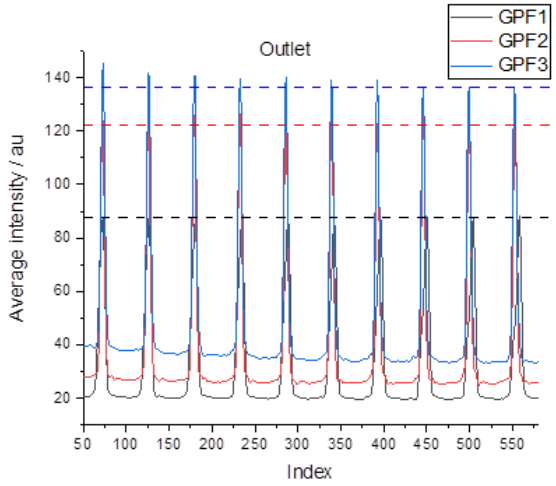

Figure 5: (Top) Inlet and (Bottom) outlet average channel intensity over a 16 mm depth, 20 x 20 mm sub-volume. The dashed horizontal lines are included to aid comparison of the average intensity for the channel walls along view direction for each filter inlet/outlet. The average intensity of the channel walls across the view direction are visible in the troughs between peaks.

Whilst these do not cover the full height of the filter as the overview scan depth profiles shown in Figure 3 do, they provide more detailed information on congruent regions of all the filters, with the trends matching those from the overview scan depth profiles. A widening of the peaks (full width half maximum, FWHM) would indicate that ash deposition is occurring on the surface of the channel walls, whilst an increase in the peak intensity (without an increase in peak width) would indicate that deposition is occurring within the channel walls. Whilst every effort was made to ensure the tilt correction of the ROI scans was precise, and the channel walls were orthogonal within the sub-volume, the manufacturing tolerance of the extrusion process has some variability, such that the channel walls are not perfectly straight (see SI Figure 1). Consequently, this causes some broadening of the line profiles displayed in Figure 5, and prohibits accurate measuring of the channel wall width from these plots (less than the resolution limit of 32.1 µm).

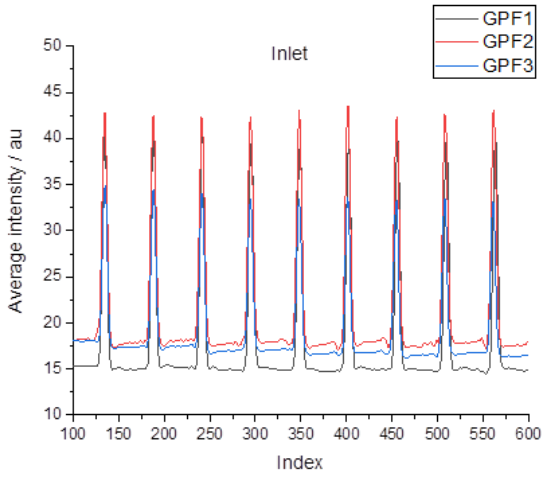

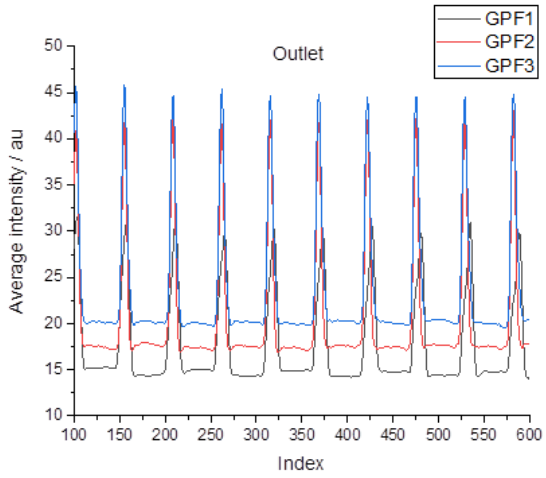

Figure 6: (Top) Inlet and (Bottom) outlet average intensity in the plug regions over a 3.2 mm depth, 20x20 mm sub-volume.

The average intensity across the channel walls however indicates that there is deposition occurring within the walls; the intensity is highest for GPF 3, and lowest for GPF 1 (baseline), and is consistent with the trends in backpressure reported in Table 4 (i.e. ash build up in the walls is directly linked to an increase in backpressure). This indicates that the use of the FBC additive reduces the amount of in-wall blocking along the channels, but does not completely negate it. The channel wall in peak intensity at the outlet for GPF 1 is significantly lower than at the inlet, more so than for GPF 2 and GPF 3, and greater than that observed by the depth profile in Figure 3. Closer inspection of the peak profile for GPF 1 shows that a shoulder is appearing and widening on the left side of each peak as the x-axis index increases (i.e. position across the ROI). This indicates that there is a slight curvature to the channel walls along parallel to the field of view (see Figure S1); the ROI's are taken at the narrow edges of the filters and so the walls curve towards the apex. A similar comparison of the average intensity over a 3.2 mm depth of the inlet/outlet plug regions was made. The plugs have uneven depths of filling within the channels, and in the outlet region of GPF 2 there is some filling of the volume above each plug caused by the accumulation of the FBC additive. Therefore, to avoid any skewing in the calculation of the intensity values of the plug region, a lesser depth of plug was used compared with their average overall depth.

The intensity of the peaks in Figure 6 (channel walls) for the inlet plug region of GPF 2 is slightly higher than GPF 1 and GPF 3, as are the troughs (plugs filling every other channel); both GPF 2 and GPF 3 have a higher intensity than the baseline, indicating that the plug regions undergo some ash build up. There is visible orange discolouration from deposition of the (oxidised) FBC additive; the higher peak intensity in Figure 6 indicates that the iron oxide is depositing in/on the channel walls as well as on/in the plugs, whilst the lube oil-derived ash appears to primarily deposit within the plugs at the inlet. At the outlet region, the profile for the baseline (GPF 1) is very similar to the inlet and has the lowest intensity of all filters – there is some asymmetry to the peaks, coupled with a decrease in intensity, moving across the filter

(increase in x-axis index) due to the channel walls not being parallel. The outlet peaks and troughs for GPF 2 are slightly lower than those at the inlet (ca. 2-4%), indicating that the deposition of iron oxide is less. This may be because the iron oxide ash is aggregating and accumulating in the channels above the plugs, having a visibly larger particle size. The profile for GPF 3 has the greatest difference, with a 20-30% increase in intensity, indicating significant deposition. Observation of cross-sections of the ROIs in the plug regions reveals a range of pore sizes and vertical cracks within the plugs, however simple line profiles do not contain enough information to compare the properties of the cracks and pores between the three filters; this requires the volume segmentation and is described in the following section.

Segmentation of channels in ROI scans

Table 5: Computed average filter channel widths and difference from the baseline filter.

Region		GPF 1 (Baseline)	GPF 2	GPF 3
Inlet	Average width / µm	1516.4	1501.3	1484.7
	Standard deviation	3.4	4.8	5.7
	Difference to baseline / µm	*0.0*	-15.1 (1%)	-31.7 (2%)
Outlet	Average width / µm	1527.4	1494.5	1483.5
	Standard deviation	2.8	3.3	4.2
	Difference to baseline / µm	*0.0*	-32.9 (2%)	-43.8 (3%)

An example of segmented channels are shown in Figure 7, with the comparison of the average channel widths shown in Table 5. GPF 1 has (1 %) wider channels at the outlet than at the inlet, consistent with the depth profile in Figure 3, and the line profiles in Figures 5 and 6. Whilst this difference is small, and is lower than the resolution of the reconstruction, it is computed from 200 separate channel volumes, with a very low standard deviation and therefore is reliable.

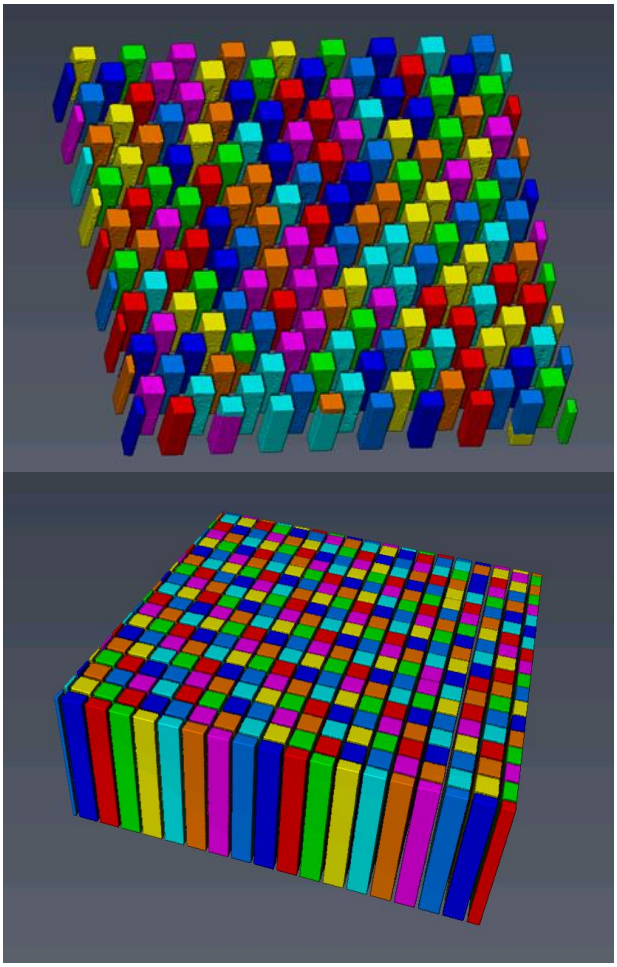

Figure 7: Example of channel segmentation in plug region (top) and in main channel region (bottom) for GPF 1. Note: incomplete channels, or those comprised of 2 segments, such as those along the left and lower edges of the inlet region (left) were not included in the analysis.

Following use, the filter channels at the inlet narrow by 1% in the case of GPF 2, and 2% for GPF 3. As was the case with the baseline GPF 1, the standard deviation of these average values is very small, and the trend is consistent across each of the 200 channels averaged. The channels narrow further at the outlets than at the inlets, with GPF 2 being 2% narrower and GPF 3 ca. 3% narrower. The greater narrowing of the channels at the outlet vs. the inlet indicates that the ash deposition is greater in these regions, and therefore indicates that the deposition for artificially doped filters begins at the outlet of the filter. The narrowing of the channel walls is directly correlated with the increase in the intensity of the depth profiles of the whole filter, and the relative changes in the line profiles from the ROIs. The lesser extent of narrowing observed for GPF 2 demonstrates and quantifies how the FBC additive beneficially impacts the performance of the filter. There is a significant 50% reduction in the channel narrowing at the inlet and a 25% reduction in the channel narrowing at the outlet, which can be directly correlated to the 40% smaller increase in the measured backpressure – i.e. use of the FBC results in the beneficial reduction in back pressure whilst maintaining the filtration efficiency improvements of ash loading (see Figure 10).

Segmentation of Plugs

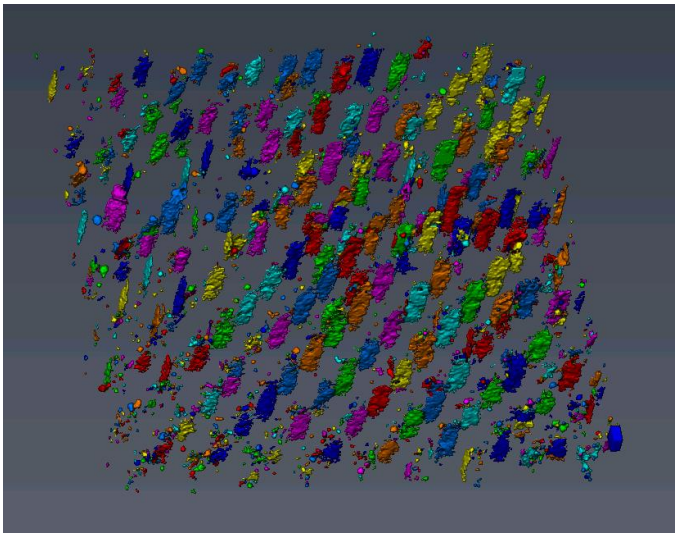

Figure 8: Example of crack and pore segmentation in the plug region. Cracks and pores occur within the filled plugs at either end of the filter.

The crack and pore concentration in the plug regions were segmented in the same manner as the channels, to investigate whether these were also being blocked/impacted by the ash. Due to the resolution limit of the measurement (ca. 32 µm), and also the detection limit/sensitivity of the segmentation, the smallest pores and cracks could not be resolved, and so the analysis reported here focuses on the medium and large features (Figures 8 and 9).

These values were sorted by surface area, volume, and anisotropy to enable separation of the channels from the cracks and pores. The outlet plug regions for GPF 2 and GPF 3 are both less porous than inlets (Figures S2 and S3), whilst for the baseline (GPF 1), the outlet plugs are more porous than the inlet (i.e. lower density). This indicates that both iron oxide and lube-derived ash are being trapped in the cracks and pores, and the blocking of these leads to an increase in filtration efficiency (Figure 10). This follows a similar trend to the channel widths and channel wall intensities from the line profile analysis. The plug region of GPF 3 was the most blocked, i.e. lowest total pore volume, ca. 40% lower than GPF 2. However, it retained the greatest number of large spherical pores; the loss of overall porosity was caused by a sharp decrease in the mid- and small-sized pores, likely as these block first with the ash.

Regarding the cracking of the plug regions, there are a greater number of cracks and pores towards the outer edge of the filter. These largely run along the edges, parallel to the walls, although the baseline GPF also has some diagonal cracks running from middle of plugs towards the walls. For all three filters, more cracks run parallel to short axis of filter than long axis (see schematic in Figure 11), and the porosity is observed to increase towards the narrow edges of the filters.

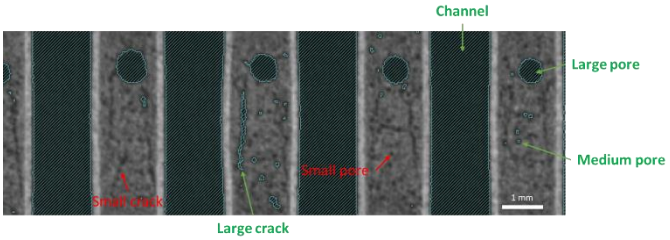

Figure 9: Example of segmentation of pores and cracks within plug regions highlighting the features that could (green) and could not (red) be reliably segmented.

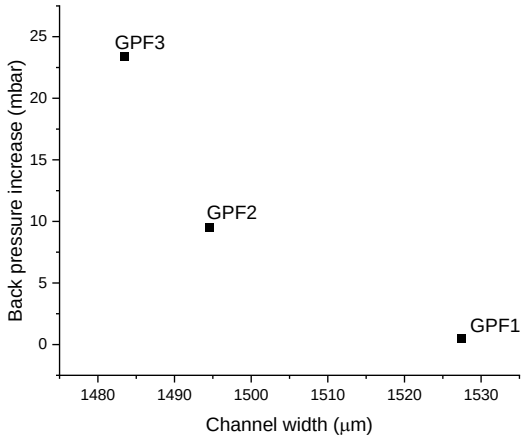

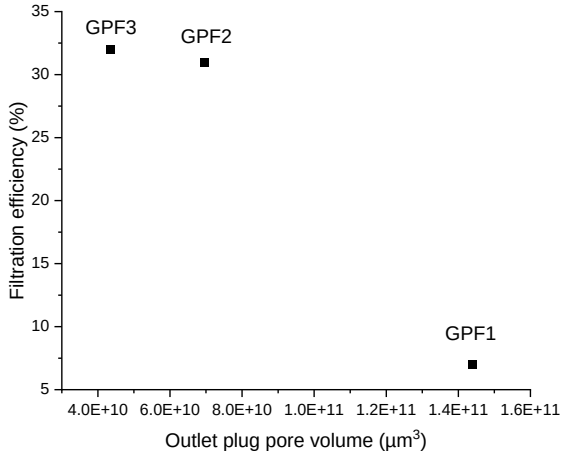

Figure 10: (Top) Correlation between average channel width and backpressure; (Bottom) Correlation of final filtration efficiency with outlet plug pore volume (operating point 1). Values are total areas/volumes summed over 200 complete channels/plugs.

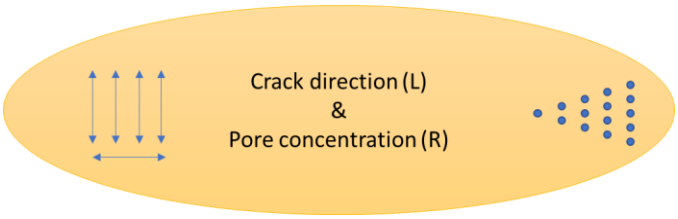

Figure 11: Schematic of pore and crack location and concentration

Conclusions

By using advanced µCT characterization and quantification, it has been possible to correlate the macroscopic performance of GPFs (i.e. backpressure and filtration efficiency) tested under real world conditions with their microscopic characteristics. Whilst many previous studies focused on single channel or small subsections tested under controlled laboratory conditions, the imaging of intact filters tested under real world conditions is an important step in understanding of GPF performance and how this can be enhanced.

Low resolution µ-CT overview scans may be used to qualitatively compare the filters, and to give an indication of where ash deposition occurs, whilst high resolution ROIs allow for direct quantification of where and how this happens, and enable correlation with the consequent effects on filter performance.

µ-CT techniques revealed that the filtration efficiency of the GPF correlates strongly with plug crack/pore filling, and suggest this may also be influenced by channel wall filling/density. The FBC derived-ash deposits on the surface of the filter inlet, and within the cracks at the outlet plugs, and hence blocks them and improves filtration efficiency. The lube oil-derived ash appeared to primarily deposit within the plugs at the inlet of the filter.

The µ-CT technique revealed that the average inlet channel diameters for GPF 3 (lube oil) were reduced by 32 µm with respect to the baseline (GPF 1), whilst GPF 2 (FBC) was reduced by 15 µm. Thus, compared to GPF 3, GPF 2 had a ~50% reduction in ash accumulation/deposition in the inlet channel. In addition, the average outlet channel diameters for GPF 3 were reduced by 44 µm and GPF 2 were reduced by 33 µm with respect to the baseline (GPF 1), indicating a 25% reduction in ash accumulation when comparing the two filters. The degree of ash deposition increases towards the outlets of both filters (GPFs 2 & 3). The lesser extent of this narrowing observed for GPF 2 demonstrates and quantifies how the FBC additive beneficially impacts the backpressure performance of the filter. To further bridge the understanding between lab testing and real world performance, the use of higher resolution µCT and chemical imaging on subsections of filter walls and plugs could be employed to investigate the distribution and impact of the FBC and on the mechanism of interaction [21, 26].

Through the test program employed, the controlled build-up of ash from both lube oil components and the FBC additive into new GPFs was achieved, and demonstrated to provide increased filtration efficiency of the filters. Using dynamometer testing it was established that the FBC additive (used in GPF 2) provided a lower backpressure increase at the same targeted ash loading as lube oil componentry (GPF 3) whilst maintaining the improved filtration efficiency. Quantification of both plug and wall structure at the inlets and outlets of the filters revealed how blocking of pores in the end plug regions of the filter directly benefits the filtration efficiency, whilst deposition on and within filter walls causes an undesired increase in backpressure, which is alleviated by the use of a FBC additive. These results indicate that FBCs may be used if ash accumulation in the GPF is desired to improve the filtration efficiency of new filters; however further testing is required to investigate the wider impact of FBCs on other engine and exhaust components.

References

1. Kotek, M., Jindra, P., Prikner, P., and Marik, J., “Comparison of PM production in gasoline and diesel engine exhaust gases,” *Agronomy Research* 15:1041-1049, 2017.
2. Demuynck, J., Favre, C., Bosteels, D., Hamje, H. et al., "Real-World Emissions Measurements of a Gasoline Direct Injection Vehicle without and with a Gasoline Particulate Filter," SAE Technical Paper 2017-01-0985, 2017, doi: https://doi.org/10.4271/2017-01-0985.
3. Karjalainen. P., Pirjola, L., Heikkila, J., Lahde, T, et al., “Exhaust particles of modern gasoline vehicles: A laboratory and an on-road study,” *Atmospheric Environment* 97:262-270, 2014, doi: https://doi.org/10.1016/j.atmosenv.2014.08.025.
4. Uy, D., Ford, M. A., Jayne, D. T., O’Neill, A. E., et al., “Characterization of gasoline soot and comparison to diesel soot: Morphology, chemistry, and wear,” *Tribology International* 80:198-209, 2014, doi: https://doi.org/10.1016/j.triboint.2014.06.009.
5. Jones, M. P., Storm, M., York, A. P. E., Hyde, T. I., et al., “4D in-situ microscopy of aerosol filtration in a wall flow filter,” *Materials* 13:5676, 2020, doi: https://doi.org/10.3390/ma13245676.
6. Shae, H., Lam, W., Remias, J., et al., “Effect of Lubricant Oil Properties on the Performance of Gasoline Particulate Filter (GPF),” *SAE Int. J. Fuels Lubr.* 9(3):650-658, 2016, doi: https://doi.org/10.4271/2016-01-2287.
7. Lambert, C., Chanko, T., Jagner, M., Hangas, J., et al., "Analysis of Ash in Low Mileage, Rapid Aged, and High Mileage Gasoline Exhaust Particle Filters," *SAE Int. J. Engines* 10(4):1595-1603, 2017, doi: https://doi.org/10.4271/2017-01-0930.
8. Sterlepper, S., Claßen, J., Pischinger, S., Cox, J., et al., “Design of a novel gasoline particulate filter aging method,” *Emiss. Control Sci. Technol.* 6:151-162, 2020, doi: https://doi.org/10.1007/s40825-019-00130-5.
9. Hua, L., Pan, J., MIAO, S., Gu, D., et al., "Effect of Ash on Gasoline Particulate Filter Using an Accelerated Ash Loading Method," SAE Technical Paper 2018-01-1258, 2018, doi: https://doi.org/10.4271/2018-01-1258.
10. Custer, N., Kamp, C. J., Sappok, A., Pakko J., et al., "Lubricant-Derived Ash Impact on Gasoline Particulate Filter Performance," *SAE International Journal of Engines* 9(3):1604-1614, 2016, doi: http://www.jstor.org/stable/26284925.
11. Twigg, M. V., Collins, N. R., Morris, D., O’Connell, T. J., et al., “The effect of phosphorus and boron lubricant oil additives on catalyst and engine durability,” *SAE Transitions* 113(4):948-959, 2004, doi: https://www.jstor.org/stable/44740816.
12. Moldovan, M., Rauch, S., Morrison, G. M., Gomez, M., et al., “Impact of ageing on the distribution of platinum group elements

and catalyst poisoning elements in automobile catalysts," *Surf. Interface. Anal*. 35:354-359, 2003, doi: 10.1002/sia.1541.
13. Brett, P. S., Neville, A. L., Preston, W. H., Williamson, J., "An investigation into lubricant related poisoning of automotive three-way catalysts and lambda sensors," *SAE Transactions* 98(4):269-280, 1989, doi: https://www.jstor.org/stable/44472029.
14. Lambert, C., Bumbaroska, M., Dobson, D., Hangas, J. et al., "Analysis of High Mileage Gasoline Exhaust Particle Filters," *SAE Int. J. Engines* 9(2):1296-1304, 2016, doi: https://doi.org/10.4271/2016-01-0941.
15. Maire, E., and Withers, P. J., "Quantitative X-ray tomography," *International Materials Reviews*, 59(1):1-43, 2013, doi: 10.1179/1743280413Y.0000000023.
16. du Plessis, A., Yadroitsev, I., Yadroitsava, I., Le Roux., S. G., "X-Ray Microcomputed Tomography in Additive Manufacturing: A Review of the Current Technology and Applications," *3D Printing and Additive Manufacturing* 5(3):227-247, 2018, doi: http://doi.org/10.1089/3dp.2018.0060.
17. Haugen, H. J., Qasim, S. B., Matinlinna, J. P., Vallittu, P., et al., "Nano-CT as tool for characterization of dental resin composites," *Scientific Reports*, 10:15520, 2020, doi: https://doi.org/10.1038/s41598-020-72599-y.
18. Blažek, M., Žalud, M., Kočí, P., York, A., et al., "Washcoating of catalytic particulate filters studied by time-resolved X–ray tomography," *Chemical Engineering Journal* 409:128057, 2021, doi: https://doi.org/10.1016/j.cej.2020.128057.
19. Nakayama, H., Banno, Y., Mochizuki, H., et al., "Development of GPF Using μ-CT Measurement and Numerical Analytical Technique," *Top Catal*. 62:419–425, 2019, doi: https://doi.org/10.1007/s11244-019-01136-7.
20. Gong, J., Stewart, M. L., Zelenyuk, A., Strzelec, A., et al., "Importance of filter's microstructure in dynamic filtration modeling of gasoline partiucalte filters (GPFs): Inhomogeneous porosity and pore size distribution," Chemical Engineering Journal 338:15-26, 2018, doi: https://doi.org/10.1016/j.cej.2018.01.006.
21. Kamp, C., Folino, P., Wang, Y., Sappok, A. et al., "Ash Accumulation and Impact on Sintered Metal Fiber Diesel Particulate
22. Filters," *SAE Int. J. Fuels Lubr*. 8(2):2015, doi:10.4271/2015-01-1012.Vamvakeros, A., Jacques, S. D. M., Di Michiel, M., et al., "5D operando tomographic diffraction imaging of a catalyst bed," *Nat. Commun.* 9:4751, 2018, doi: https://doi.org/10.1038/s41467-018-07046-8.
23. Price, S. W. T., Martin, D. J., Parsons, A. D., Sławiński, W. A., et al., "Chemical imaging of Fischer-Tropsch catalysts under operating conditions," *Science Advances* 3, 2017, doi: 10.1126/sciadv.1602838.
24. Price, S. W. T., Geraki, K., Ignatyev, K., Witte, P. T., et al., "In Situ Microfocus Chemical Computed Tomography of the Composition of a Single Catalyst Particle During Hydrogenation of Nitrobenzene in the Liquid Phase," *Angew. Chem.* 127:10024-10027, 2015, doi: https://doi.org/10.1002/ange.201504227.
25. Sappok, A., Wang, Y., Wang, R., Kamp, C. et al., "Theoretical and Experimental Analysis of Ash Accumulation and Mobility in Ceramic Exhaust Particulate Filters and Potential for Improved Ash Management," *SAE Int. J. Fuels Lubr*. 7(2):2014, doi:10.4271/2014-01-1517.
26. Yang, J., Stewart, M., Maupin, G., Herling, D., and Zelenyuk, A., "Single wall diesel particulate filter (DPF) filtration efficiency studies using laboratory generated particles," *Chemical Engineering Science* 64:1625-1634, 2009, doi: 10.1016/j.ces.2008.12.011.
27. Campenon, T., Wouters, P., Blanchard, G., Macaudiere, P. et al., "Improvement and Simplification of DPF System Using a Ceria-based Fuel-borne Catalyst for Diesel Particulate Filter Regeneration in Serial Applications," SAE Technical Paper 2004-01-0071, 2004, doi: https://doi.org/10.4271/2004-01-0071.
28. Stępień, Z., Ziemiański, L., Żak, G., Wojtasik, M., et al., "The evaluation of fuel borne catalyst (FBC's) for DPF regeneration," *Fuel* 161:278-286, 2015, doi: https://doi.org/10.1016/j.fuel.2015.08.071.
29. Song, J., Wang, J., and Boehman, A. L., "The role of fuel-borne catalyst in diesel particulate oxidation behavior," *Combustion and Flame*, 146(1–2):73-84, 2006, doi: https://doi.org/10.1016/j.combustflame.2006.03.012.
30. Hoekman, S. Kent, and Leland, A., "Literature Review on the Effects of Organometallic Fuel Additives in Gasoline and Diesel Fuels.," *SAE International Journal of Fuels and Lubricants* 11(1):105-24, 2018, doi: https://www.jstor.org/stable/26554699.
31. Caprotti, R., Field, I., Michelin, J., Schuerholz, S. et al., "Development of a Novel DPF Additive," SAE Technical Paper 2003-01-3165, 2003, doi: https://doi.org/10.4271/2003-01-3165.
32. Dallanegra, R. and Caprotti, R., "Validation of Fuel Borne Catalyst Technology in Advanced Diesel Applications," SAE Technical Paper 2014-01-1401, 2014, doi: https://doi.org/10.4271/2014-01-1401.
33. Caprotti, R., Dallanegra, R., and Dahai, J., "Fuel Borne Catalyst Assisted Diesel Particulate Filter Regeneration in Current and Legacy Retrofitted Vehicles in China," SAE Technical Paper 2015-01-2017, 2015, doi: https://doi.org/10.4271/2015-01-2017.
34. Schindelin, J., Arganda-Carreras, I., Frise, E., Kaynig, V., et al., "Fiji: an open-source platform for biological-image analysis," *Nature Methods* 9(7):676–682, 2019, doi:10.1038/nmeth.
35. Limaye, A., "Drishti: a volume exploration and presentation tool. Proc. SPIE 8506, Developments in X-Ray Tomography VIII, 85060X" 2012.

Contact Information

Removed for submission

Acknowledgments

Removed for submission

Definitions/Abbreviations

DPF	Diesel particulate filter
FBC	Fuel borne catalyst
GPF	Gasoline particulate filter
μ-CT	X-ray micro computed tomography

Appendix

Additional information on the additives used in this study:

The active ingredient of the fuel borne catalyst is a stabilised iron oxide colloid. This additive typically used in diesel fuel applications and is present during the combustion of diesel fuel, where the iron oxide becomes entrained in the resulting soot. Here it acts as a catalyst to reduce the temperature of the soot oxidation, thus enabling DPF regeneration to occur at lower temperatures. An iron oxide FBC was chosen for this study as this is the most common commercial FBC material (iron oxide and ferrocene being typical examples).

Calcium is a common metal component found in ash, as a result of calcium-containing additives being used in the vehicles lube oil and was thus deemed appropriate for this study. The lube oil contained in the vehicle system matched that used to dose the fuel. For this study, in order to reduce the complexity, additional common lube oil metal species such as zinc or magnesium so that during analysis we were able to compare one type of ash to another. The comparison of different lube oil components was beyond the scope of this study.

Further Information on GPF Commissioning Studies:

Measurements:

The particulate number and particulate mass were measured before and after the GPF on the test bench, using Particle Counter and Microsoot (DMS 500 Measurement) analysis techniques. The particle counter used for the measurements was the AVL particle counter: APC 489. This works according to the principle of a condensation particle counter. Three measuring points were added to exhaust systems before and after the GPF: one each for particle counter, pressure and temperature measurements.
The GPFs examined had approximately a 1.5 L volume. Each GPF was firstly benchmarked on an engine test bed, to establish the initial, baseline GPF filtration efficiency, prior to testing. A pre-defined test cycle was used to collate this data, which included a regeneration period, to remove any carbonaceous material, followed by the three steady state operating points:

Table S1: Operating points and regeneration procedure for GPFs

Operating Point	**Information**
Initial Heating Period	Engine speed steadily increased up to 3000 rpm/200 Nm. [0 – 585 seconds]
GPF Regeneration	Operating point of 3500 rpm/250 Nm held [585 – 1495 seconds]
Operating Point 1	5500 rpm/300 Nm operating point held [1495 – 3598 seconds]
Operating Point 2	3500 rpm/150 Nm operating point held [3598 – 3893 seconds]
Operating Point 3	1500 rpm/50 Nm operating point held [3893 – 4199 seconds]
GPF Regeneration	Operating point of 3500 rpm/250 Nm held [4199 – 5107 seconds]
Cool to end of cycle	Ramp down, end of test at 5158 seconds

This test cycle was repeated, providing average data values that represented the filtration efficiency of each GPF when they were new and unused, at each operating point. This gave a baseline for comparison once testing had been carried out.

Each GPF used was purchased at the same time from the same vendor and displayed highly similar structural dimensions – however some natural variation between each filter, due to manufacturing tolerances is to be expected and is unavoidable. Thus we assessed the initial filtration efficiency of

each individual filter and took an average of two back-to-back assessments as the overall result. The filtration efficiency was calculated using the following equation, and so is based on particulate number before and after the GPF:

((particulate number before GPF – particulate number after GPF)/particulate number before GPF)*100%.

The particulate numbers used above were taken every 0.1 seconds and averaged across the operating point total measurements/time.

Table S2 details the full breakdown of filtration efficiency results (reported in Table 3) including standard deviation, calculated from the Run 1 and Run 2 data.

Table S2: Individual and average filtration efficiency measurements at initial and final stage for GPFs at each operating point

Operating Point 1									
GPF	Initial Filtration Efficiency (stage 1) Run 1	Initial Filtration Efficiency (stage 1) Run 2	Average Initial Filtration Efficiency	Initial Filtration Efficiency std. dev	Final Filtration Efficiency (stage 3) Run 1	Final Filtration Efficiency (stage 3) Run 2	Average Final Filtration Efficiency	Final Filtration Efficiency std. dev	Increase
1	53	49	51	2	57.5	58	57.75	0.25	7
2	47	47	47	0	78.5	78	78.25	0.25	31
3	49	47	48	1	80.5	80	80.25	0.25	32
Operating Point 2									
GPF	Initial Filtration Efficiency (stage 1) Run 1	Initial Filtration Efficiency (stage 1) Run 2	Average Initial Filtration Efficiency	Initial Filtration Efficiency std. dev	Final Filtration Efficiency (stage 3) Run 1	Final Filtration Efficiency (stage 3) Run 2	Average Final Filtration Efficiency	Final Filtration Efficiency std. dev	Increase
1	65	65	65	0	73	72.5	72.75	0.25	8
2	62	64	63	1	89	89	89	0	26
3	64	62	63	1	91.5	92	91.75	0.25	29
Operating Point 3									
GPF	Initial Filtration Efficiency (stage 1) Run 1 (%)	Initial Filtration Efficiency (stage 1) Run 2 (%)	Average Initial Filtration Efficiency (%)	Initial Filtration Efficiency std. dev	Final Filtration Efficiency (stage 3) Run 1 (%)	Final Filtration Efficiency (stage 3) Run 2 (%)	Average Final Filtration Efficiency (%)	Final Filtration Efficiency std. dev	Increase (%)
1	71	71	71	0	79	79.5	79.25	0.25	8
2	68	73	71	3	93.5	93	93.25	0.25	22
3	68.5	67.5	68	1	94	95	94.5	0.5	27

Vehicle Assessments:

For vehicle testing, the standard 3-way catalytic converter was located directly after the exhaust gas turbocharger in a separate small housing, approx. 0.5 – 1 m in front of the particle filter.

Further information on the real-driving cycle used to assess the GPF (Stage 2 – Commissioning):

- Once the fuel tank was filled with the appropriate fuel (GPF 1: gasoline only, GPF 2: FBC additive, GPF 3: lube additive) the vehicle was driven around a pre-defined route in Landau, Germany, mimicking real driving
- Distance per GPF approx. 800km with 68 L fuel Aral Super Plus RON 98 (one complete tank)
- One RDE trip had approx. 92km; divided into 38% city section, 31% rural and 31% highway
- The average driving time per route was approx. 1:50h, total per GPF approx. 15h

Further information on fuel dosing:

Once the GPF baseline filtration efficiency had been assessed using the test cycle, the GPF was mounted into position on a BMW 530i Touring (2 L inline 4-cylinder gasoline direct injection (GDI) engine, power 185 kW, torque 350 Nm, curb weight 1715 kg, fuel tank capacity 68 L). This vehicle was chosen as it has a GPF and GDI engine. The lube oil in the vehicle was changed, to match that of the additive package componentry.

Upon the installation of the GPF, the fuel tank was filled with gasoline fuel (Aral Super Plus RON 98). The filling of the fuel tank was altered during each assessment:

GPF 1: 68 L Gasoline fuel only, for baseline testing

GPF 2: Fuel dosed with FBC additive

GPF 3: Fuel dosed with lube additives

To effectively dose the additives into the fuel, the following method was used: 34 L gasoline added to fuel tank, pre-mixed additive in 5 L fuel added, following which the tank was filled to capacity.

The FBC treat rate was calculated, using the iron content of the FBC additive, and the relative mass of ash that is obtained. Through understanding the volume of GPF and targeted g/L of ash desired, the total g of iron oxide ash was known, and this could be used to calculate the amount of FBC additive to bring about this ash amount.

GPF 3 was treated with a complete lubricant additive package. This comparative example represented the prior art solution of dosing the fuel with formulated lubricating oil, but was modified by the exclusion of the lubricating base-oil to avoid the other negative effects of heavy hydrocarbons (such as gummy deposits on engine critical surfaces) which might otherwise interfere with the interpretation of results. Thus, the test in GPF 3 focused on the impact of ash deposition from the complete lubricant additive package that was added to the test base fuel.

TGA (thermogravimetric analysis) was used to establish the ash content of the lubricant additive package for dosing purposes, with the residue % remaining being representative of the oxidised ash content. TGA was carried out using the following test method: An additive sample was analysed to determine the thermal stability within a typical TGA apparatus under an atmosphere of air. 10mg of sample was heated at 10°C/min between 30 and 825 °C under a flow of 50ml/min air. The pans used were Platinum. At 825 °C it is assumed that only ash from the additives remain.

Table S3: µ-CT scan parameters for each type conducted on filters 1-3: x-ray beam peak accelerating voltage, kVp and power, W; Source to object distance (SOD), mm; Source to detector distance (SDD), mm; detector binning (Bin.); analogue gain of detector signal, dB; exposure (Exp.) time, ms; number of projection images acquired throughout 360° rotation with 2 or 4 frames averaged per projection; and reconstructed voxel resolution, µm.

Scan Type	Peak Voltage (kVp)	Power (W)	SOD (mm)	SDD (mm)	Bin.	Analogue gain (dB)	Exp. time (ms)	Proj. / FPP	Voxel Resolution (µm)
Overview	200	47	504	861	2	12	125	1571 / 2	234.4
Additional overview	160	45	281	800	1	18	134	4401 / 4	70.3
ROI	180	32	128	798	1	24	134	5001 / 4	32.1

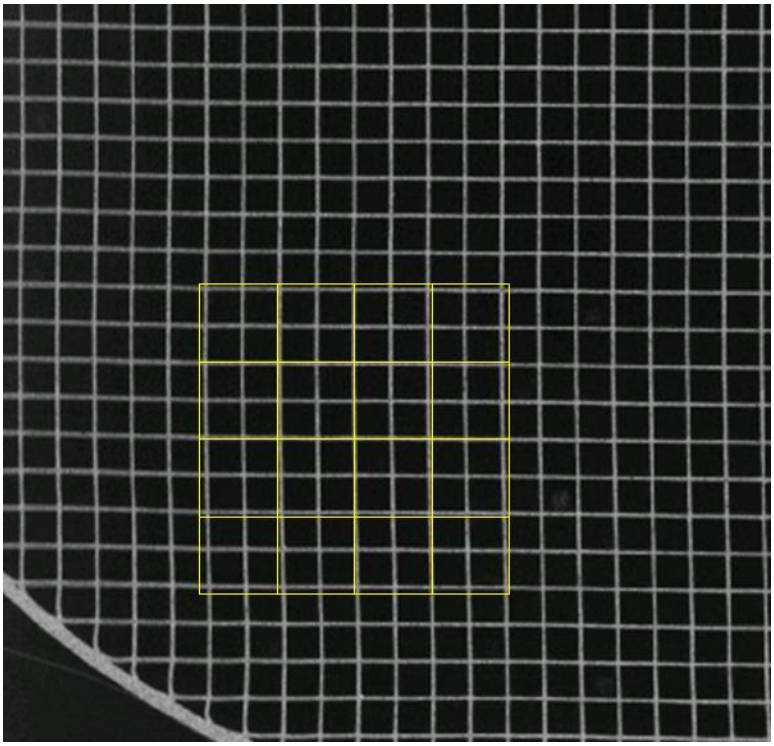

Figure S1: Non-parallel nature of channel walls

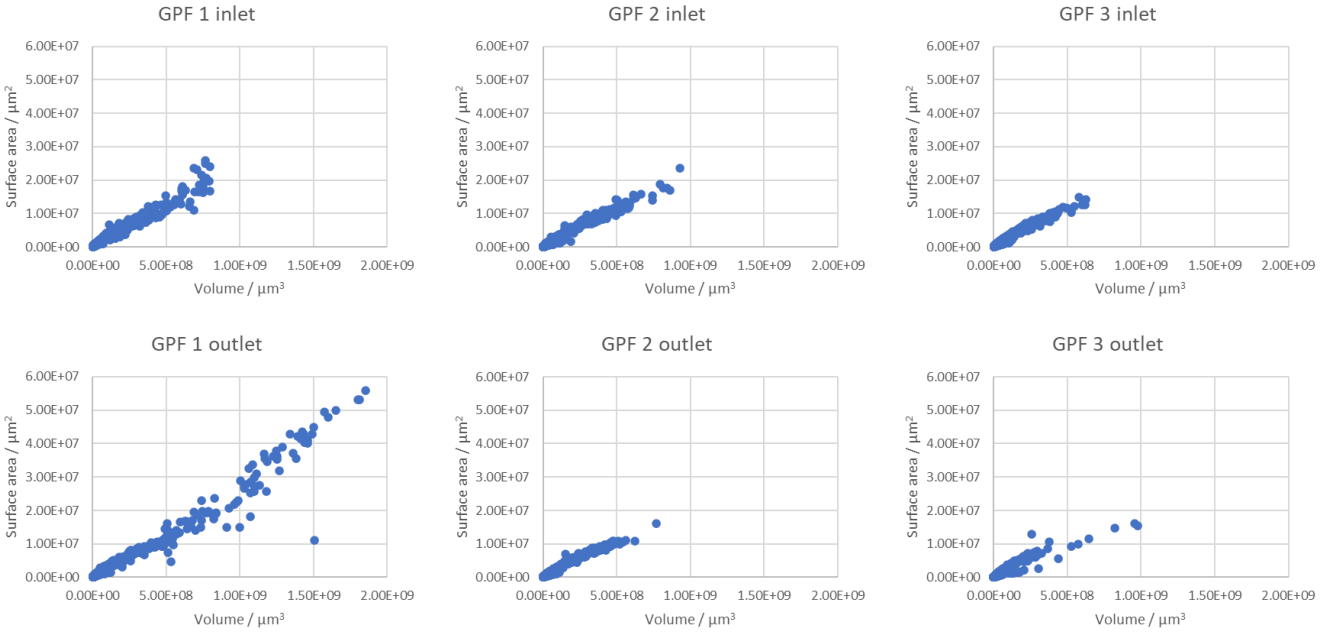

Figure S2: Plug pore and crack analysis

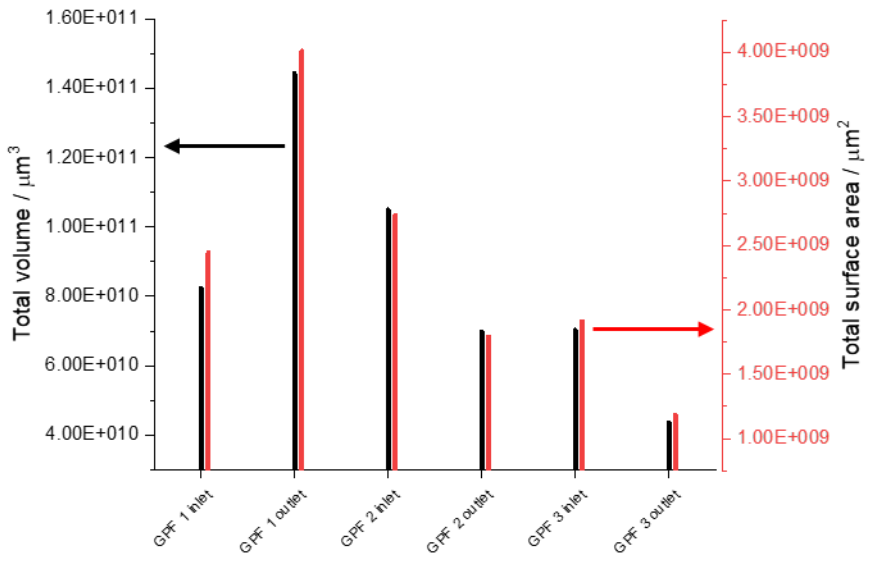

Figure S3: Calculated total pore and crack volume, and surface area for the GPFs